

pubs.acs.org/JPCL Letter

Crystal Structure of $Au_{30-x}Ag_x(S-tBu)_{18}$ and Effect of the Ligand on Ag Alloying in Gold Nanomolecules

Kalpani Hirunika Wijesinghe, Naga Arjun Sakthivel, Tanya Jones, and Amala Dass*



Cite This: J. Phys. Chem. Lett. 2020, 11, 6312-6319



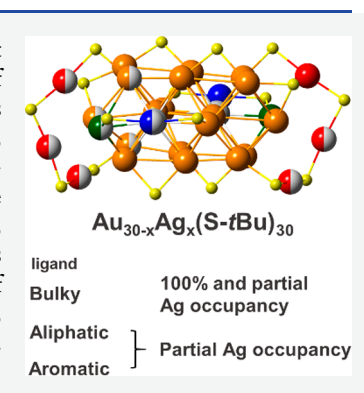
ACCESS

Metrics & More

Article Recommendations

Supporting Information

ABSTRACT: We report the X-ray crystal structure of the $Au_{30-x}Ag_x(S-tBu)_{18}$ alloy and the effect of the ligand on alloying site preferences. Gold—silver nanoalloys prepared by co-reduction of metal salts are known to have only partial Ag occupancies. Interestingly, $Au_{30-x}Ag_x(S-tBu)_{18}$ has 100% Ag occupancy at two sites on the core surface as well as partial Ag occupancies on the surface, capping, and staples sites. The $Au_{30-x}Ag_x(S-tBu)_{18}$ (x=1-5) composition was confirmed by X-ray diffraction and electrospray ionization mass spectrometry studies. Thiolate ligands can be categorized into three classes on the basis of the groups at the α -position as aliphatic, aromatic, and bulky thiols. The effect of the ligand on Ag doping can be clearly seen in the crystal structures of $Au_{36-x}Ag_x(SPh-tBu)_{24}$ and $Au_{38-x}Ag_x(SCH_2CH_2Ph)_{24}$ when compared with that of $Au_{30-x}Ag_x(S-tBu)_{18}$. Ag is preferentially doped onto the core surface when the ligand is aliphatic, and Ag is doped in both core surface and staple metal sites when the ligand is aromatic or bulky.



old nanomolecules are atomically monodisperse nano $oldsymbol{ extstyle J}$ particles having a precise number of gold atoms and thiolate ligands, such as Au₂₅(SR)₁₈, Au₃₀(SR)₁₈, Au₃₆(SR)₂₄, and Au₃₈(SR)₂₄. ¹⁻⁴ Moreover, these molecules are stable under ambient conditions, and in powder and solution forms in nonpolar solvents. The molecular composition of nanomolecules can be determined by mass spectrometry with electrospray ionization mass spectrometry (ESI-MS) and matrix-assisted laser desorption ionization (MALDI) MS and from single-crystal X-ray diffraction (SC-XRD).⁵ A nanomolecule's structure is composed of a metallic core protected by a ligand shell containing staple metal sites and thiolate ligands. The metallic core is composed of core-centered atoms, without Au-S bonds and a core surface where Au atoms are protected by sulfur atoms. The staple motifs are identified on the basis of the number of gold sites in a motif, for example, monomeric (-S-Au-S-), dimeric (-S-Au-S-Au-S-), and trimeric (-S-Au-S-Au-S-Au-S-) staples. The nanoscale size and optical and electronic properties of nanomolecules are interesting as they offer applications in a wide array of areas, such as catalysis, biosensing, and drug delivery.6-15

The commonly used thiolate ligands for the synthesis of gold nanomolecules (AuNMs) can be categorized into three groups, namely, aliphatic (i.e., *n*-butanethiol and phenylethanethiol), aromatic (i.e., thiophenol), and bulky ligands (i.e., *tert*-butyl thiol and adamantanethiol). The bulkiness and properties of the ligands govern the structure, size, and electrochemical and optical properties of the nanomolecule. In the case of aromatic ligands, both aromaticity and bulkiness have an influence on the structure and size of the nanomolecule. The sulfur atoms of the bulky ligands are bound to a tertiary

carbon atom drives the electron density toward the sulfur atom and forms stronger Au–S bonds. In addition, a steric effect of the *tert*-butyl group plays a major role by hindering the growth of the nanomolecule. Therefore, the *tert*-butyl-S ligand-protected AuNM series is limited to a few sizes: $Au_{23}(SR)_{16}$, $Au_{30}(SR)_{18}$, $Au_{46}(SR)_{24}$, and $Au_{65}(SR)_{29}$. $Au_{23}(SR)_{16}$, $Au_{46}(SR)_{24}$, and $Au_{65}(SR)_{29}$.

Alloying nanomolecules with foreign metal atoms offers another dimension of tunability. AuNMs can be doped with different foreign metal atoms, such as Ag, Pd, Pt, Mn, Cu, etc., to form nanoalloys.^{7,26–34} Nanoalloys show different physicochemical properties compared to those of their parent compounds.^{35–38} A significant amount of literature on nanoalloys with aliphatic and aromatic classes of ligands exists.^{23,32,37,39–42} However, only a few AuNM-based nanoalloys have been prepared using bulky ligands.

Here, we report the crystal structure of a bulky thiolated nanoalloy, $\mathrm{Au_{30-x}Ag_x(S-tBu)_{18}}$, deduced by X-ray crystallography. The composition was determined by mass spectrometry and corroborates the SC-XRD-based composition. The Ag doping pattern observed in this structure is unprecedented, where Ag is occupied 100% as well as partially on the surface metal sites, whereas other reported Au-based nanoalloys prepared by co-reduction of metal salts have only partial occupancies. For example, $\mathrm{Au_{25-x}Ag_x(SR)_{18}}$, $\mathrm{Au_{36-x}Ag_x(SR)_{24}}$, and $\mathrm{Au_{38-x}Ag_x(SR)_{24}}$ have Ag partial occupancies in the ranges

Received: April 30, 2020 Accepted: July 15, 2020 Published: July 23, 2020





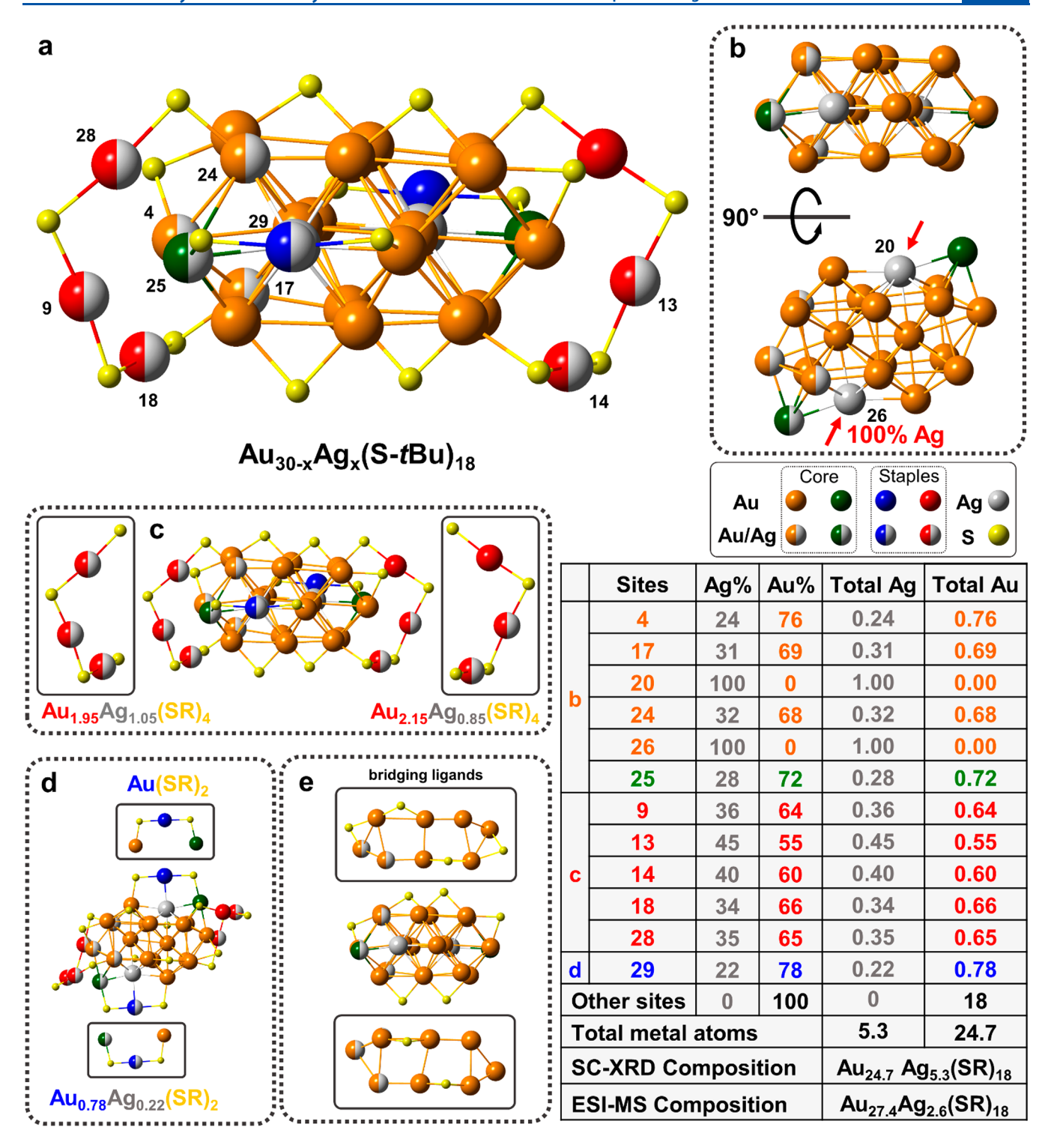


Figure 1. X-ray crystal structure of the $Au_{30-x}Ag_x(S-tBu)_{18}$ nanoalloy (ball-and-stick model). (a) $Au_{30-x}Ag_x(S-tBu)_{18}$ with 18 Au sites, 10 partially occupied Au/Ag sites, and two Ag sites contributing a total of $Au_{24.7}$ and $Ag_{5.3}$. (b) Bicuboctahedral 20-atom core with two capping atoms, where 16 sites are Au, two sites are Ag (sites 20 and 26), and four sites are partially occupied by Au and Ag. (c) Monomeric staples, where one site is partially occupied by Au/Ag. (d) Trimeric staples, where five sites are partially occupied by Au/Ag. (e) Bridging thiolate groups on the bicuboctahedral core. The site-based compositions are listed in the table. The site numbers are assigned as they are in the crystallographic information file (CIF). Carbon and hydrogen atoms and some staple—metal to core—metal bonds have been omitted for the sake of clarity. A generic layer-by-layer composition-based formula for the $Au_{30-x}Ag_x(S-tBu)_{18}$ nanoalloy can be written as $M_2@M_{18}(SR)_6@M_2@[M_2(SR)_4]-[M_6(SR)_8]$ corresponding to core center M_2 @ core surface M_{18} protected by six bridging ligands @ M_2 capping atoms @ $M_2(SR)_4$ monomeric staples @ $M_6(SR)_8$ trimeric staples, where M represents metal sites. The layer-by-layer composition is $Au_2@Au_{15.13}Ag_{2.87}(SR)_6@Au_{1.72}Ag_{0.28}@[Au_{1.78}Ag_{0.22}(SR)_4][Au_{4.1}Ag_{1.9}(SR)_8]$. The central sites are solely occupied by Au. The core surface is occupied by $Au_{1.513}$ and $Ag_{2.87}$. Capping sites are occupied by $Au_{4.1}Ag_{1.9}$.

of 45-61%, 11-56%, and 28-52%, respectively. 43-45 Also, we discuss the effect of aliphatic, aromatic, and bulky ligands on Ag doping in AuNMs prepared by co-reduction of metal salts.

In the bulky, tert-butylthiolated AuNM series, green gold, $Au_{30}(S-tBu)_{18}$, is a remarkably stable compound that has been discovered with two different compositions to date: Au₃₀(S $t\mathrm{Bu})_{18}$ and $\mathrm{Au}_{30}\mathrm{S}(\mathrm{S}\text{-}t\mathrm{Bu})_{18}$. These nanomolecules have a similar core structure with a minor difference in the thiolate monolayer from the additional sulfur atom. In another bulky ligand, adamantanethiolate (S-Adm), a compound with a similar composition, Au₃₀(S-Adm)₁₈ has been discovered. However, it has an entirely different crystal structure with a hexagonal close-packed Au₁₈ core, protected by six dimeric staples.²² Although Au₃₀(S-Adm)₁₈ and Au₃₀(S-tBu)₁₈ have the same number of Au atoms and ligands, which are tertiary thiols, their crystal structures are very different because of the difference in the bulkiness of the carbon tail.

 $Au_{30-x}Ag_x(S-tBu)_{18}$ crystallized in monoclinic space group $P2_1/n$. The crystal structure was refined to an R_1 value of 11.7% at 1.1 Å resolution (Table S1). $Au_{30-x}Ag_x(S-tBu)_{18}$ has a structural framework similar to that of its parent compound, $Au_{30}(S-tBu)_{18}$ (Figure 1). It has a 22-metal atom core in a face centered cubic (FCC) configuration with 20 atoms arranged to form the bicuboctahedral core. An interpenetrating bicuboctahedron resembles a rod-like structure. It has two center atoms, four edge atoms, 14 vertices, and 14 facets: two rectangular, four trapezoidal, four triangular, and four square facets. The ends of the core have two square and two triangular facets, and rectangular and trapezoidal facets are arranged along the length of the structure. One square facet at each end of the core is capped by a μ_4 metal atom. Altogether, this makes the 22-metal atom core. The eight remaining metal atoms are in staple motifs. Two monomeric staples are located on either side of the elongated axis of the bicuboctahedron, protecting the capping and vertex metal sites. The six remaining metal atoms are arranged in two trimeric staples with eight thiolates (-S-Au-S-Au-S-Au-S-) at the ends of the bicuboctahedron. The six remaining thiolate ligands are distributed as bridging ligands. Figure 1 shows the details of the $Au_{30-x}Ag_x(S-tBu)_{18}$ crystal structure. Au_{30-x}Ag_x(S-tBu)₁₈ is a chiral molecule, and the enantiomers are shown in Figure S1. Figure S2 compares the monometallic $Au_{30}(S-tBu)_{18}$ and $Au_{30}S(S-tBu)_{18}$ structures with that of $Au_{30-x}Ag_x(S-tBu)_{18}$. Figure S3 shows the orientations of the ligand around the $Au_{30-x}Ag_x(S-tBu)_{18}$

The Ag atoms are doped at three different places in $Au_{30-x}Ag_r(S-tBu)_{18}$: (i) at five sites on the bicuboctahedral surface (54.5% of the total Ag), (ii) at one capping μ_4 atom site (5.3% of the total Ag), and (iii) on staples, one monomeric staple site (4.2% of the total Ag) and five sites on the trimeric staples (36% of the total Ag). The partial occupancy of Au/Ag is due to the substitutional disorder of Au and Ag (Figure 1). The core Au–Au average bond length is 2.946 ± 0.197 Å, and the core Au-Ag average bond length is 2.780 ± 0.041 Å. The core Au-S bond (2.397 \pm 0.145 Å) is slightly longer than the partially occupied core Au/Ag-S bond (2.348 ± 0.032 Å). This trend is also observed in the staples: Au-S (2.295 \pm 0.013 Å) and partially occupied Au/Ag-S (2.238 \pm 0.162 Å) (Tables S2 and S3).

The two central atoms are solely Au; i.e., the occupancy factor is 1.00. This observation is consistent with the earlier predictions that incorporation of Ag at the center of the core is energetically unfavorable.⁴³ Among 18 surface metal sites on

the core, two sites are 100% occupied by Ag and three sites are partially occupied by Ag. The three partially occupied sites have the following Au/Ag occupancies: Au4/Ag4, 76%/24%; Au17/ Ag17, 69%/31%; and Au24/Ag24, 68%/32%. Five doped sites on the core contribute to 2.87Ag in the overall composition. The 100% Ag occupied sites are Ag20 and Ag26. These two sites are symmetrical vertices on the core surface, adjacent to the capping atoms, and are buried under the monomeric staple metal atoms. Those core surface atoms seem to be favorable sites for being replaced by foreign Ag atoms. The capping site has a Ag partial occupancy: Au25/Ag25, 72%/28%. Of the two monomeric staples, only one site is partially occupied by Ag: Au29/Ag29, 78%/22%. In trimeric staples, five metal sites are partially occupied by Ag contributing 1.90Ag to the total composition. They are distributed as follows: Au9/Ag9, 64%/ 34%; Au13/Ag13, 55%/45%; Au14/Ag14, 60%/40%; Au18/ Ag18, 66%/34%; and Au28/Ag28, 65%/35%. The overall composition from the X-ray crystal structure is Au_{24.7}Ag_{5.3}(StBu)₁₈. ESI-MS of $Au_{30-x}Ag_x(S-tBu)_{18}$ reveals that x ranges from 1 to 5 and it is consistent with the composition observed via SC-XRD (vide infra).

In a recent work, Fortunelli et al. reported a computational study of energy analysis to determine the preferred Ag doping sites on Au₃₀(SR)₁₈.⁴⁷ They categorized the preferred Ag doping sites into five groups: (1) two sites where Ag doping is optimal or most favorable, (2) 14 sites where doping is less favorable $(5-8 k_B T)$, (3) two sites where doping is less favorable with a slightly higher energy of 9.5 k_BT , (4) 10 sites where the energy is higher $(12-14 k_B T)$, and (5) two sites where doping is most unfavorable (19 k_BT).⁴⁷ The $Au_{30-x}Ag_x(S-tBu)_{18}$ experimental structure from this work has two sites that are 100% occupied by Ag. Those two 100% Ag sites are the sites computationally predicted to be optimal Ag doping sites by Fortunelli et al. (Table S4).

Figure 1 reports the $Au_{30-x}Ag_x(SR)_{18}$ structure as a ball-andstick model. The size and shape of the atoms in this model are idealized. It does not correlate the experimental data and the refined structure model; i.e., there is no indicator to assess for the correct or incorrect assignment of atoms in the model. In the thermal ellipsoid model (Figure 2), the electron density of appropriate atoms in the refined structure model is indicated by the size and shape of the ellipsoids, which is an indicator of the anisotropic displacement parameter (ADP). The size and shape of the thermal ellipsoid reveal whether an atom assignment is correct or incorrect.⁴⁴ The unusually large or small size of the atoms indicates discrepancy in the model or an incorrect assignment. The ADP value shows atoms as larger ellipsoids, if lighter element is incorrectly assigned as a heavier element in the model.⁴⁸ Initially, sites 20 and 26 were assigned as Au sites (Figure S4). The ellipsoid size with the Au assignment instead of Ag is larger than the other metal sites (Figure S4), as the electron density of Au (79 electrons) is higher than that of Ag (47 electrons). Substitutional disorder refinement was performed to determine the Ag% partial occupancy (see Experimental Methods for details) and revealed Ag occupancy >90% in both sites (95% Ag for site 20 and 98% Ag for site 26). The two sites were then assigned as Ag only, and the ADP value decreases; i.e., the ellipsoid size and shape became smaller and similar to those of the other metal sites (Figure S4b). The thermal ellipsoid model represents the agreement between the structure model and the experimental data and should ideally be shown in all X-ray crystal structure reports in the field.

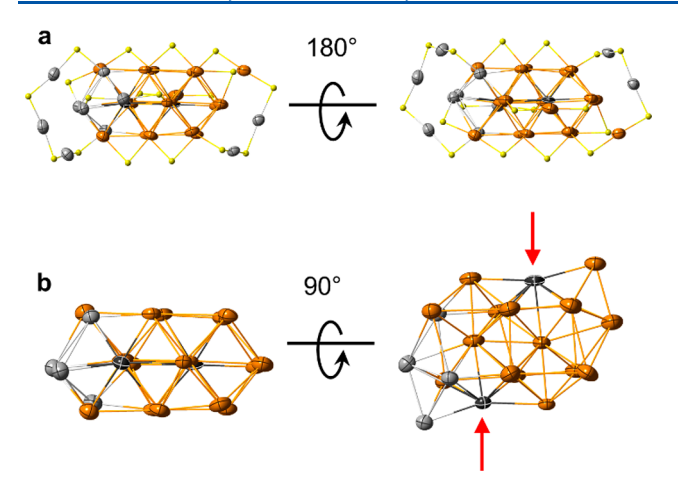


Figure 2. X-ray structure of the $Au_{30-x}Ag_x(S-tBu)_{18}$ nanoalloy in a thermal ellipsoid model: 100% Au sites, orange; 100% Ag sites, dark gray; Au/Ag partially occupied sites, light gray; sulfur, yellow. (a) Au_{30-x}Ag_xS₁₈ view. (b) Twenty-two-atom core (100% Ag sites are marked by red arrows). The metal sites are displayed as thermal ellipsoids to demonstrate the equally sized and shaped ellipsoids of metal sites in the model. The thermal ellipsoid size and shape are indicators of the anisotropic displacement parameter (ADP) value that is used to identify the occupancy factor in heterometal substitute sites. These values of ellipsoid size and shape are calculated from the experimental data, which reveals the electron density of the given atom. If the atoms are incorrectly assigned, the ellipsoid shape and size would be unusually large or small (Figure S4). The ball-and-stick model is an idealized way to represent the structure and provides no correlation to the atom assignment with experimental data. Therefore, a thermal ellipsoid model should be reported along with other models in X-ray crystal structure reports.

The composition of $Au_{30-x}Ag_x(S-tBu)_{18}$ was determined by ESI-MS (Figure S5). The number (x) of Ag doping ranges from 1 to 5, consisting of five different AuAg nanoalloy species: $Au_{25}Ag_5$, $Au_{26}Ag_4$, $Au_{27}Ag_3$, $Au_{28}Ag_2$, and $Au_{29}Ag_1$. The m/zpeaks of the +1 charge state for these species were observed at 7069, 7158, 7247, 7336, and 7425 Da, respectively. The difference between the two adjacent peaks is 89 Da, which is the atomic mass difference between Au and Ag. The +2 charge state m/z peaks were observed for Au₂₆Ag₄ (3579 Da), Au₂₇Ag₃ (3624 Da), Au₂₈Ag₂ (3668 Da), and Au₂₉Ag₁ (3713 Da) species. The relative Ag contributions of each species (Au₂₅Ag₅, Au₂₆Ag₄, Au₂₇Ag₃, Au₂₈Ag₂, and Au₂₉Ag₁) are 0.15, 0.50, 1.01, 0.89, and 0.06, respectively. The Ag contribution from each species to the total composition was calculated using their relative peak heights.

The average composition of the AuAg nanoalloy was calculated to be Au_{27.38}Ag_{2.62}(S-tBu)₁₈ from the mass spectrum. The average composition from ESI-MS data is different from the SC-XRD composition of Au_{24.7}Ag_{5.3}(S-tBu)₁₈, which could be due to the difference in the ionization efficiency of the various species of nanoalloys in mass spectrometry.

The SC-XRD structure was modeled with two 100% Ag atom sites (Figure 1). Therefore, in the $Au_{30-x}Ag_x(SR)_{18}$ compound, one would expect the value of x to start at 2, but the mass spectrometry data revealed the existence of a $Au_{29}Ag_1(S-tBu)_{18}$, i.e., x = 1, species. In the SC-XRD structure, we modeled the two sites (20 and 26) with Ag partial occupancy of >90% as 100% Ag sites, as ≤10% Au partial occupancy may not be reliably modeled. Therefore, the $Au_{29}Ag_1(S-tBu)_{18}$ species could exist in small amounts. The

intensity of the peak corresponding to the Au₂₉Ag₁ species in the mass spectra is very low (Figure S5), and its relative Ag contribution to the total composition is 0.06, which agrees with the observation from the SC-XRD data.

AuNMs alloyed with Ag prepared by co-reduction of metal salts have shown only partial Ag occupancies, to date. 43-45 Guidez et al. computationally predicted Ag doping on central atoms in $Au_{25-n}Ag_n(SH)_{18}$ to be highly unfavorable and the core surface sites are preferred. 49 The Au_{25-x}Ag_x(SCH₂CH₂Ph)₁₈ nanoalloy prepared by co-reduction of metal salts revealed that Ag atoms were partially occupied on the vertices of the icosahedral core, and central and dimeric staple metal sites were exclusively Au. 43 Other studies also indicate that the central core atoms are exclusively Au. 43-45,50 Jin et al. reported that Ag can be doped onto the surface and staple motifs of Au_{25-x}Ag_x(SCH₂CH₂Ph)₁₈⁻, using a structural transformation process by reacting Au₂₃(Scyclohexane)₁₆ with the Ag(1)-(SCH₂CH₂Ph) polymeric precursor.⁵⁰ It has 100% Ag occupancy at one site on the icosahedral shell, and the partial Ag occupancy is between 82% and 93%. Six sites on the staple motifs have 100% Ag occupancy, and other sites have partial Ag occupancy ranging from 45% to 50%.

Notably, the doping patterns in other metal-based alloys (doped with Au, Cu, Pt, Pd, etc.) are different from those of AuNM-based alloys. For example, 100% Au occupancy in the central atom has been observed in [Ag₂₄Au(SR)₁₈]^{-.5} However, in the case of silver doping in Au₂₅, Ag has not been doped on the central metal atom (see above). 43,50 In another case, the Au-doped Ag₄₄ compound with a formula of $[M_{12}Ag_{32}(SR)_{30}]^{4-}$, where M represents either Ag or Au, has 12 100% Au occupied sites. Au doping was observed in the icosahedral core. The M_{12} core is then fully face capped by 20 Ag atoms to form the second shell. 23,27,52 These results indicate that the doping patterns observed in other metalbased alloys are different from those of AuNM-based alloys with Ag.

The thiolate ligand group (i.e., aliphatic, aromatic, or bulky) determines the structure and physiochemical properties of the nanoalloys. The bulky ligand-protected $Au_{30-x}Ag_x(S-tBu)_{18}$ structure is compared with the previously published aliphatic-like ligand-protected Au_{38-x}Ag_x(SCH₂CH₂Ph)₂₄ and aromatic ligand-protected Au_{36-x}Ag_x(SPh-tBu)₂₄ structures (Figure 3). The aliphatic-like ligand-protected Au_{38-x}Ag_x(SCH₂CH₂Ph)₂₄ structure has a 23-atom face-shared biicosahedral core, protected by six dimeric and three monomeric staples (Figure 3). The core has two central atoms and 21 vertex atoms. The central two atoms are only Au, and nine sites on the core surface are partially occupied by Ag atoms. The nine sites are distributed as three sets of three atoms along the length of the rod-like core; three atoms on each end of the rod and remaining three atoms are located at face-shared atoms between two icosahedra (Figure 3). Ag is not incorporated at staple metal sites, and they are exclusively occupied by Au (Figure 3).45

In the aromatic ligand, the $Au_{36-x}Ag_x(SPh-tBu)_{24}$ structure has an FCC core made of 28 metal atoms protected by four dimeric staples and 12 bridging ligands (Figure 3).44 The 28atom core can be viewed as four interpenetrating cuboctahedra with four tetrahedral center atoms. It can also be viewed as cris-cross stacking of two bicuboctahedra [as in $Au_{30}(S-tBu)_{18}$]. The four central atoms are solely occupied by Au (Figure 3). Of 24 core surface atoms, four vertex atoms are symmetrically

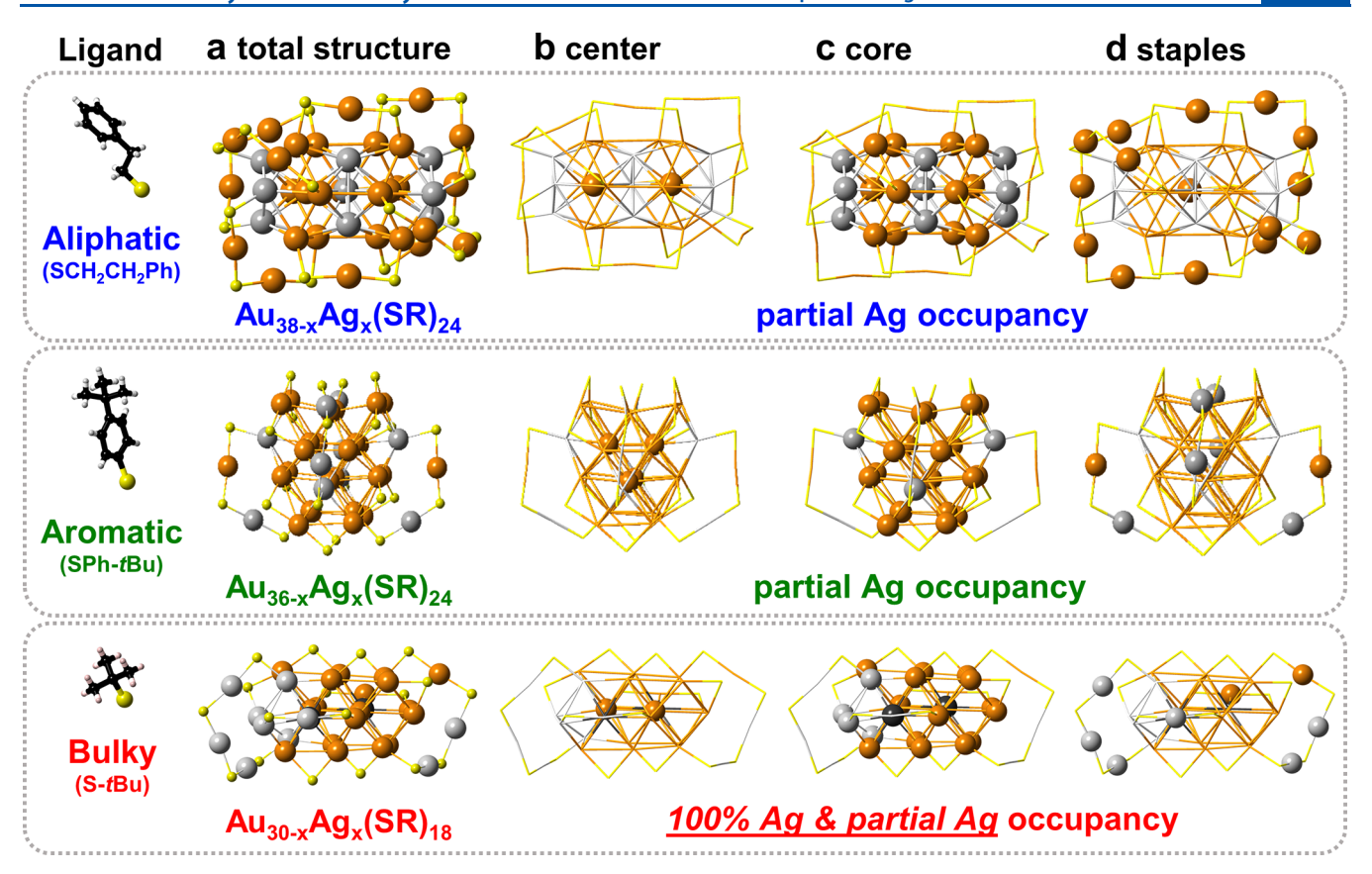


Figure 3. Comparison of aliphatic, aromatic, and bulky ligated $Au_{38-x}Ag_x(SCH_2CH_2Ph)_{24}$, $Au_{36-x}Ag_x(SPh-tBu)_{24}$, and $Au_{30-x}Ag_x(S-tBu)_{18}$ alloy nanomolecules, respectively. The structures of the respective ligands are shown on the left. (a) Crystal structures with the staples and bridging thiolate ligands: 100% Au sites, orange; 100% Ag sites, dark gray; Au/Ag partially occupied sites, light gray; sulfur, yellow. C and H atoms have been omitted for the sake of clarity. (b) Central core atoms 100% occupied by Au. (c) Core surface atoms (central core atoms have been omitted for the sake of clarity). $Au_{38-x}Ag_x$ and $Au_{36-x}Ag_x$ have partial Ag occupancy. $Au_{30-x}Ag_x$ has two sites with 100% Ag and four sites with partial Ag occupancy. (d) Staple atoms of the three structures. $Au_{38-x}Ag_x$ has no Ag-occupied sites. In $Au_{36-x}Ag_x$, six symmetrical sites are partially occupied by Ag, and in $Au_{30-x}Ag_x$, six sites are asymmetrically (partially) occupied by Ag. Staple metal—core metal bonds have been omitted for the sake of clarity in panels a—d.

doped by Ag with partial occupancy (at the ends rod-like bicuboctahedra) (Figure 3). Also, Ag is partially doped on the six symmetric sites of the dimeric staples (Figure 3). Interestingly, Au_{30-x}Ag_x(S-tBu)₁₈ prepared by co-reduction of metal salts has both 100% Ag occupancies and partial Ag occupancies (surface and staples).

The Ag doping pattern in AuAg nanoalloy structures protected by aliphatic and aromatic ligands exhibits symmetrically doped Ag sites [Au_{38-x}Ag_x(SCH₂CH₂Ph)₂₄ and $Au_{36-x}Ag_x(SPh-tBu)_{24}$]. Surprisingly, bulky ligated Au_{30-x}Ag_x(S-tBu)₁₈ exhibits both symmetrical and asymmetrical Ag doping patterns. The 100% Ag sites are symmetrically doped, whereas partial Ag occupancy sites are asymmetrically doped. Independent of the ligand type, all three compounds show no Ag occupancy on the central core atoms, confirming it is the energetically unfavorable site for Ag occupancy. In the aliphatic ligand [Au_{38-x}Ag_x(SCH₂CH₂Ph)₂₄], all of the Ag atoms are doped onto only the core surface sites, but in aromatic and bulky ligands $[Au_{36-x}Ag_x(SPh-tBu)_{24}]$ and $Au_{30-x}Ag_x(S-tBu)_{24}$ tBu)₁₈], Ag atoms are doped onto core surface as well as staple metal sites. Overall, the extents of Ag occupancy on the core surface for aliphatic, aromatic, and bulky ligands are 100%, ~70%, and ~60%, respectively. In aromatic and bulky ligands, the remaining ~30% and ~40%, respectively, are distributed on the staple metal sites.

The average core Au-Au bond distances in $Au_{38}(SCH_2CH_2Ph)_{24}$, $Au_{36}(SPh-tBu)_{24}$, $Au_{30}(S-tBu)_{18}$, and their corresponding nanoalloys (Au_{38-x}Ag_x, Au_{36-x}Ag_x, and Au_{30-x}Ag_x, respectively) are not significantly different (Table S2). In the core, the average bond length between Au and Au/ Ag partially occupied sites is shorter in bulky ligated Au_{30-x}Ag_x $(2.796 \pm 0.168 \text{ Å})$ compared to the aliphatic and aromatic ligated nanoalloys $[Au_{38-x}Ag_x (2.848 \pm 0.081 \text{ Å}) \approx Au_{36-x}Ag_x$ $(2.844 \pm 0.096 \text{ Å})]$ (Table S2). In Au_{30-x}Ag_x, the average bond distance is shortened around Ag-doped sites (2.796 ± 0.168 Å), compared to the monometallic Au-Au bond distances (2.897 \pm 0.179 Å). The staple Au-S bond lengths in the $Au_{38-x}Ag_{xy}$ $Au_{36-x}Ag_{xy}$ and $Au_{30-x}Ag_{x}$ nanoalloys are shorter than those of their monometallic structures (Table S2), whereas core metal—S bond lengths of monometallic structures are slightly shorter than those of their nanoalloy counterparts. Also, bulky ligated Au_{30-x}Ag_x has a shorter staple Au/Ag partially occupied site-S bond length (2.238 ± 0.162 Å) compared to that of aromatic ligated $Au_{36-x}Ag_x$ (2.312 \pm 0.012 Å).

In summary, the X-ray crystal structure of $Au_{30-x}Ag_x(S-tBu)_{18}$ has revealed unprecedented details about the Ag doping pattern for compounds prepared by co-reduction of metal salts. The central atoms are exclusively Au occupied, and core surface sites have both 100% Ag and partial Ag occupancies.

Also, the structure has both *symmetrical and asymmetrical doping patterns* (for 100% Ag and partial Ag occupancies, respectively). The experimental discovery of the two 100% Ag sites in $\text{Au}_{30-x}\text{Ag}_x(\text{S-}t\text{Bu})_{18}$ confirms the computational prediction by Fortunelli et al., which indicated that those sites are optimal for Ag occupancy.⁴⁷ The overall crystallographic composition was found to be $\text{Au}_{24.7}\text{Ag}_{5.3}(\text{S-}t\text{Bu})_{18}$, and the ESI-MS composition was found to be $\text{Au}_{27.4}\text{Ag}_{2.6}(\text{S-}t\text{Bu})_{18}$. ESI-MS qualitatively validates the SC-XRD composition by revealing that the Ag ranges from 1 to 5; i.e., $\text{Au}_{30-x}\text{Ag}_x(\text{S-}t\text{Bu})_{18}$ is a combination of five species: $\text{Au}_{25}\text{Ag}_5$, $\text{Au}_{26}\text{Ag}_4$, $\text{Au}_{27}\text{Ag}_3$, $\text{Au}_{28}\text{Ag}_2$, and $\text{Au}_{29}\text{Ag}_1$.

The investigation of doping patterns in aliphatic, aromatic, and bulky ligand-protected nanoalloys has revealed some interesting trends in the effect of the ligand on the Ag doping preference. Ag is preferably doped on the core surface in the following order: aliphatic > aromatic > bulky ligands. Ag doping occurred in the staples, as well, when the ligand is aromatic or bulky. Also, SC-XRD data indicate Ag doping in ${\rm Au_{30-x}Ag_x}$ shortens the bond length around the corresponding sites on the core, compared to the monometallic AuNMs.

EXPERIMENTAL METHODS

Materials. Tetrachloroauric(III) acid (HAuCl₄·3H₂O, Alfa-Aesar, 99%), silver nitrate (AgNO₃, Fisher chemicals, 99%), 2-methyl-2-propanethiol (tBuSH, Acros, 99%), and sodium tetrahydridoborate (NaBH₄, Acros Organics, 99%) were used. HPLC grade solvents tetrahydrofuran (THF), THF-butylated hydroxytoluene (THF-BHT), toluene, and methanol were used. All of the items were used as received. Bio-Rad-SX1 beads (Bio-Rad) were used for size exclusion chromatography.

Synthesis. The synthesis of $Au_{30-x}Ag_x(S-tBu)_{18}$ was carried out in two steps. First, 100 mg of HAuCl₄·3H₂O and 18 mg of AgNO₃ were dissolved in 15 mL of THF and reacted with 29 μ L of tBuSH in a round-bottom flask [(AuAg):thiol ratio of 1:0.7]. The mixture was stirred vigorously for 15 min (450 rpm). Then, 113 mg of NaBH₄ dissolved in cold water was added to the reaction mixture. The solution turned black, indicating the formation of nanoparticles. Stirring was continued for 1 h. Then, the solution was rotary evaporated to remove the excess solvent. The product was washed with methanol and water to remove byproducts, and finally, the crude product was extracted with toluene. In the second step, the crude was etched with excess tBuSH at 70 °C while being stirred for 12 h. The etched product was rotary evaporated to dryness; the product was washed with methanol and water to remove the byproducts, and the etched product was extracted with toluene. The etched product was further separated by size exclusion chromatography (using THF-BHT as the solvent) to obtain pure $Au_{30-x}Ag_x(S-tBu)_{18}$. Single crystals were grown by vapor diffusion of methanol into a toluene solution of $Au_{30-x}Ag_x(S-tBu)_{18}$.

Instrumentation. ESI-MS was performed using a Waters Synapt HDMS instrument using THF as the solvent. SC-XRD data were collected at the Advanced Light Source (beamline 11.3.1), Lawrence Berkeley National Laboratory. The black crystal was isolated and mounted on MiTeGen kapton loops and placed in a 100(2) K nitrogen cold stream provided by an Oxford Cryostream 800 plus low-temperature apparatus on the goniometer head of a Bruker D8 diffractometer, equipped with a PHOTON 100 CMOS detector operating in a shutterless mode. The diffraction data were collected using synchrotron

radiation at a wavelength of 0.7293 Å, and the data were corrected for absorption effects using the multiscan method.⁵³

Crystal Structure. $C_{60}Ag_{5.26}Au_{24.74}S_{18}$; formula weight of 6737.58; monoclinic; space group $P2_1/n$; a=25.1222 (10) Å; b=14.9693 (6) Å; c=40.2014 (19) Å; $\alpha=90^\circ$; $\beta=99.435^\circ$ (3); $\gamma=90^\circ$; volume of 14913.7 (11) ų; Z=4; $\rho_{calc}=3.001$ cm³; $\mu=26.716$ mm⁻¹; F(000)=11398; 2θ range of $4.03-38.202^\circ$; 73664 reflections collected; 11227 independent ($R_{int}=0.1015$); $R_1=0.1176$; $wR_2=0.2819$ [$I\geq 2\sigma(I)$]; for all data $R_1=0.1518$; $wR_2=0.3089$.

Substitutional Disorder Refinement. The $(AuAg)_{30}$ crystal structure was subjected to substitutional refinement to obtain a reliable model. The structure was determined by using SHELXT, and the structure model was refined using SHELXL least-squares methods in the Olex2 program. All metal sites and S atoms (except the S18 site) were refined anisotropically.

First, all of the metal sites were assigned as Au in the structure solution. Then, one Au atom was selected at a time, and in the Olex interface, the partial occupancy command was entered as "EXYZ Au Ag" and refined. ⁵⁴ The EXYZ command also adds the EADP for the corresponding sites. This was repeated for all 30 Au atoms. After several cycles of refinement, sites with ≥90% Ag/Au occupancy are converted back to Ag/Au only sites. The thermal ellipsoid model of the metal sites in the final structure model is shown in Figure 2.

As noted above, the crystal structure was determined to a resolution of $\sim\!\!1.1$ Å (at $\theta_{\rm max}=19.101^\circ).$ It is pertinent to further elaborate here that the crystal diffracted to $\sim\!\!0.82$ Å; however, only a few (weak) reflections were observed beyond $\sim\!\!1.1$ Å resolution. To conserve the quality of the structure model, the data was truncated to a $\theta_{\rm max}$ of 19.101°. The quality of the data was sufficient for the identification of metal and sulfur sites, and to model the alloy structure and composition reliably. The minimum resolution was not ideal to model all of the carbon atoms and to add hydrogens. However, the substitutional disorder refinement of Au and Ag was not affected by the $\sim\!\!1.1$ Å resolution limit, as the structural model is the spatial average obtained by integrating all of the recorded reflections.

ASSOCIATED CONTENT

Supporting Information

The Supporting Information is available free of charge at https://pubs.acs.org/doi/10.1021/acs.jpclett.0c01330.

ESI mass spectra, alternate crystal structure view, atomic coordinates, anisotropic displacement parameters, bond lengths, bond angles, and atomic occupancies for ${\rm Au_{30-x}Ag_x(S-tBu)_{18}~(PDF)}$

Crystallographic data (CCDC 2007624) (CIF)

AUTHOR INFORMATION

Corresponding Author

Amala Dass — Department of Chemistry and Biochemistry, University of Mississippi, Oxford, Mississippi 38677, United States; occid.org/0000-0001-6942-5451; Email: amal@olemiss.edu

Authors

Kalpani Hirunika Wijesinghe — Department of Chemistry and Biochemistry, University of Mississippi, Oxford, Mississippi 38677, United States; Ocid.org/0000-0002-7049-0370

Naga Arjun Sakthivel — Department of Chemistry and Biochemistry, University of Mississippi, Oxford, Mississippi 38677, United States; Oorcid.org/0000-0001-8134-905X

Tanya Jones — Department of Chemistry and Biochemistry, University of Mississippi, Oxford, Mississippi 38677, United States

Complete contact information is available at: https://pubs.acs.org/10.1021/acs.jpclett.0c01330

Notes

The authors declare no competing financial interest.

ACKNOWLEDGMENTS

National Science Foundation Grant CHE-1808138 supported this work. The authors gratefully acknowledge Dr. Kevin Gagnon and Dr. Simon Teat for their help with SC-XRD data collection. This research used resources of the Advanced Light Source, which is a U.S. Department of Energy Office of Science User Facility operated under Contract DE-AC02-05CH11231.

REFERENCES

- (1) Dass, A.; Stevenson, A.; Dubay, G. R.; Tracy, J. B.; Murray, R. W. Nanoparticle MALDI-TOF Mass Spectrometry without Fragmentation: Au₂₅(SCH₂CH₂Ph)₁₈ and Mixed Monolayer Au₂₅(SCH₂CH₂Ph)_{18-x}(L)_x. J. Am. Chem. Soc. **2008**, 130, 5940-5946.
- (2) Crasto, D.; Dass, A. Green Gold: Au₃₀(S-t-C₄H₉)₁₈ Molecules. J. Phys. Chem. C **2013**, 117, 22094–22097.
- (3) Nimmala, P. R.; Dass, A. Au₃₆(SPh)₂₃ Nanomolecules. *J. Am. Chem. Soc.* **2011**, *133*, 9175–9177.
- (4) Jimenez, V. L.; Georganopoulou, D. G.; White, R. J.; Harper, A. S.; Mills, A. J.; Lee, D.; Murray, R. W. Hexanethiolate Monolayer Protected 38 Gold Atom Cluster. *Langmuir* **2004**, *20*, 6864–6870.
- (5) Whetten, R. L.; Khoury, J. T.; Alvarez, M. M.; Murthy, S.; Vezmar, I.; Wang, Z. L.; Stephens, P. W.; Cleveland, C. L.; Luedtke, W. D.; Landman, U. Nanocrystal Gold Molecules. *Adv. Mater.* **1996**, 8, 428–433
- (6) Wang, A.-Q.; Chang, C.-M.; Mou, C.-Y. Evolution of Catalytic Activity of Au–Ag Bimetallic Nanoparticles on Mesoporous Support for CO Oxidation. *J. Phys. Chem. B* **2005**, *109*, 18860–18867.
- (7) Qian, H.; Jiang, D.; Li, G.; Gayathri, C.; Das, A.; Gil, R. R.; Jin, R. Monoplatinum Doping of Gold Nanoclusters and Catalytic Application. *J. Am. Chem. Soc.* **2012**, *134*, 16159–16162.
- (8) Murugadoss, A.; Okumura, K.; Sakurai, H. Bimetallic AuPd Nanocluster Catalysts with Controlled Atomic Gold Distribution for Oxidative Dehydrogenation of Tetralin. *J. Phys. Chem. C* **2012**, *116*, 26776–26783.
- (9) Boisselier, E.; Astruc, D. Gold Nanoparticles in Nanomedicine: Preparations, Imaging, Diagnostics, Therapies and Toxicity. *Chem. Soc. Rev.* **2009**, *38*, 1759–1782.
- (10) Bunz, U. H. F.; Rotello, V. M. Gold Nanoparticle—Fluorophore Complexes: Sensitive and Discerning "Noses" for Biosystems Sensing. *Angew. Chem., Int. Ed.* **2010**, *49*, 3268–3279.
- (11) Saha, K.; Agasti, S. S.; Kim, C.; Li, X.; Rotello, V. M. Gold Nanoparticles in Chemical and Biological Sensing. *Chem. Rev.* **2012**, *112*, 2739–2779.
- (12) Bowman, M.-C.; Ballard, T. E.; Ackerson, C. J.; Feldheim, D. L.; Margolis, D. M.; Melander, C. Inhibition of HIV Fusion with Multivalent Gold Nanoparticles. *J. Am. Chem. Soc.* **2008**, *130*, 6896–6897
- (13) Brown, S. D.; Nativo, P.; Smith, J.-A.; Stirling, D.; Edwards, P. R.; Venugopal, B.; Flint, D. J.; Plumb, J. A.; Graham, D.; Wheate, N. J. Gold Nanoparticles for the Improved Anticancer Drug Delivery of the Active Component of Oxaliplatin. *J. Am. Chem. Soc.* **2010**, *132*, 4678–4684.
- (14) Chaki, N. K.; Tsunoyama, H.; Negishi, Y.; Sakurai, H.; Tsukuda, T. Effect of Ag-Doping on the Catalytic Activity of Polymer-

- Stabilized Au Clusters in Aerobic Oxidation of Alcohol. *J. Phys. Chem.* C 2007, 111, 4885–4888.
- (15) Pengo, P.; Şologan, M.; Pasquato, L.; Guida, F.; Pacor, S.; Tossi, A.; Stellacci, F.; Marson, D.; Boccardo, S.; Pricl, S.; Posocco, P. Gold Nanoparticles with Patterned Surface Monolayers for Nanomedicine: Current Perspectives. *Eur. Biophys. J.* **2017**, *46*, 749–771.
- (16) Rambukwella, M.; Sakthivel, N. A.; Delcamp, J. H.; Sementa, L.; Fortunelli, A.; Dass, A. Ligand Structure Determines Nanoparticles' Atomic Structure, Metal-Ligand Interface and Properties. *Front. Chem.* **2018**, *6*, 330.
- (17) Jones, T. C.; Sumner, L.; Ramakrishna, G.; Hatshan, M. b.; Abuhagr, A.; Chakraborty, S.; Dass, A. Bulky *t*-Butyl Thiolated Gold Nanomolecular Series: Synthesis, Characterization, Optical Properties, and Electrocatalysis. *J. Phys. Chem. C* **2018**, *122*, 17726–17737.
- (18) Tlahuice-Flores, A.; Whetten, R. L.; Jose-Yacaman, M. Ligand Effects on the Structure and the Electronic Optical Properties of Anionic Au₂₅(SR)₁₈ Clusters. *J. Phys. Chem. C* **2013**, *117*, 20867–20875.
- (19) Kurashige, W.; Niihori, Y.; Sharma, S.; Negishi, Y. Precise Synthesis, Functionalization and Application of Thiolate-Protected Gold Clusters. *Coord. Chem. Rev.* **2016**, 320–321, 238–250.
- (20) Pei, Y.; Gao, Y.; Zeng, X. C. Structural Prediction of Thiolate-Protected Au₃₈: A Face-Fused Bi-Icosahedral Au Core. *J. Am. Chem. Soc.* **2008**, *130*, 7830–7832.
- (21) Dass, A.; Jones, T.; Rambukwella, M.; Crasto, D.; Gagnon, K. J.; Sementa, L.; De Vetta, M.; Baseggio, O.; Aprà, E.; Stener, M.; Fortunelli, A. Crystal Structure and Theoretical Analysis of Green Gold Au₃₀(S-tBu)₁₈. Nanomolecules and Their Relation to Au₃₀S(S-tBu)₁₈. J. Phys. Chem. C **2016**, 120, 6256–6261.
- (22) Higaki, T.; Liu, C.; Zeng, C.; Jin, R.; Chen, Y.; Rosi, N. L.; Jin, R. Controlling the Atomic Structure of Au₃₀ Nanoclusters by a Ligand-Based Strategy. *Angew. Chem., Int. Ed.* **2016**, 55, 6694–6697.
- (23) Zhang, X.; Yang, H.-Y.; Zhao, X.-J.; Wang, Y.; Zheng, N.-F. The Effects of Surface Ligands and Counter Cations on the Stability of Anionic Thiolated $M_{12}Ag_{32}$ (M = Au, Ag) Nanoclusters. *Chin. Chem. Lett.* **2014**, 25, 839–843.
- (24) Hesari, M.; Workentin, M. S. Facile Synthesis of Au₂₃(SC-(CH₃)₃)₁₆ Clusters. *J. Mater. Chem. C* **2014**, *2*, 3631–3638.
- (25) Yang, H.; Wang, Y.; Edwards, A. J.; Yan, J.; Zheng, N. High-Yield Synthesis and Crystal Structure of a Green Au₃₀ Cluster Co-Capped by Thiolate and Sulfide. *Chem. Commun.* **2014**, *50*, 14325–14327.
- (26) Kumara, C.; Dass, A. (AuAg)₁₄₄(SR)₆₀ Alloy Nanomolecules. *Nanoscale* **2011**, *3*, 3064–3067.
- (27) Yang, H.; Wang, Y.; Huang, H.; Gell, L.; Lehtovaara, L.; Malola, S.; Häkkinen, H.; Zheng, N. All-Thiol-Stabilized Ag₄₄ and Au₁₂Ag₃₂ Nanoparticles with Single-Crystal Structures. *Nat. Commun.* **2013**, *4*, 2422.
- (28) Niihori, Y.; Kurashige, W.; Matsuzaki, M.; Negishi, Y. Remarkable Enhancement in Ligand-Exchange Reactivity of Thiolate-Protected Au₂₅ Nanoclusters by Single Pd Atom Doping. *Nanoscale* **2013**, *5*, 508–512.
- (29) Negishi, Y.; Igarashi, K.; Munakata, K.; Ohgake, W.; Nobusada, K. Palladium Doping of Magic Gold Cluster $Au_{38}(SC_2H_4Ph)_{24}$: Formation of $Pd_2Au_{36}(SC_2H_4Ph)_{24}$ with Higher Stability than $Au_{38}(SC_2H_4Ph)_{24}$. Chem. Commun. **2012**, 48, 660–662.
- (30) Zhou, M.; Cai, Y. Q.; Zeng, M. G.; Zhang, C.; Feng, Y. P. Mn-Doped Thiolated Au₂₅ Nanoclusters: Atomic Configuration, Magnetic Properties, and a Possible High-Performance Spin Filter. *Appl. Phys. Lett.* **2011**, *98*, 143103.
- (31) Negishi, Y.; Munakata, K.; Ohgake, W.; Nobusada, K. Effect of Copper Doping on Electronic Structure, Geometric Structure, and Stability of Thiolate-Protected Au₂₅ Nanoclusters. *J. Phys. Chem. Lett.* **2012**, *3*, 2209–2214.
- (32) Zhang, B.; Bürgi, T. Doping Silver Increases the Au₃₈(SR)₂₄ Cluster Surface Flexibility. *J. Phys. Chem. C* **2016**, 120, 4660–4666.
- (33) Jin, R.; Nobusada, K. Doping and Alloying in Atomically Precise Gold Nanoparticles. *Nano Res.* **2014**, *7*, 285–300.

- (34) Du, W.; Kang, X.; Jin, S.; Liu, D.; Wang, S.; Zhu, M. Different Types of Ligand Exchange Induced by Au Substitution in a Maintained Nanocluster Template. *Inorg. Chem.* **2020**, *59*, 1675–1681.
- (35) Dass, A.; Sakthivel, N. A.; Jupally, V. R.; Kumara, C.; Rambukwella, M. Plasmonic Nanomolecules: Electrochemical Resolution of 22 Electronic States in $\mathrm{Au_{329}(SR)_{84}}$. ACS Energy Lett. **2020**, 5, 207–214.
- (36) Yan, J.; Su, H.; Yang, H.; Malola, S.; Lin, S.; Häkkinen, H.; Zheng, N. Total Structure and Electronic Structure Analysis of Doped Thiolated Silver $[MAg_{24}(SR)_{18}]^{2-}$ (M = Pd, Pt) Clusters. *J. Am. Chem. Soc.* **2015**, *137*, 11880–11883.
- (37) Alkan, F.; Pandeya, P.; Aikens, C. M. Understanding the Effect of Doping on Energetics and Electronic Structure for Au₂₅, Ag₂₅, and Au₃₈ Clusters. *J. Phys. Chem. C* **2019**, 123, 9516–9527.
- (38) Wang, S.; Li, Q.; Kang, X.; Zhu, M. Customizing the Structure, Composition, and Properties of Alloy Nanoclusters by Metal Exchange. *Acc. Chem. Res.* **2018**, *51*, 2784–2792.
- (39) Conn, B. E.; Atnagulov, A.; Bhattarai, B.; Yoon, B.; Landman, U.; Bigioni, T. P. Synthetic and Postsynthetic Chemistry of M₄Au_xAg_{44-x}(p-MBA)₃₀ Alloy Nanoparticles. *J. Phys. Chem. C* **2018**, 122, 13166–13174.
- (40) Yao, C.; Chen, J.; Li, M. B.; Liu, L.; Yang, J.; Wu, Z. Adding Two Active Silver Atoms on Au_{25} Nanoparticle. *Nano Lett.* **2015**, *15*, 1281–1287.
- (41) Bootharaju, M. S.; Chang, H.; Deng, G.; Malola, S.; Baek, W.; Häkkinen, H.; Zheng, N.; Hyeon, T. Cd₁₂Ag₃₂(SePh)₃₆: Non-Noble Metal Doped Silver Nanoclusters. *J. Am. Chem. Soc.* **2019**, *141*, 8422–8425.
- (42) Dou, X.; Yuan, X.; Yao, Q.; Luo, Z.; Zheng, K.; Xie, J. Facile Synthesis of Water-Soluble Au_{25-x}Ag_x Nanoclusters Protected by Mono- and Bi-Thiolate Ligands. *Chem. Commun.* **2014**, *50*, 7459–7462.
- (43) Kumara, C.; Aikens, C. M.; Dass, A. X-Ray Crystal Structure and Theoretical Analysis of $Au_{25-x}Ag_x(SCH_2CH_2Ph)_{18}^-$ Alloy. *J. Phys. Chem. Lett.* **2014**, *5*, 461–466.
- (44) Sakthivel, N. A.; Stener, M.; Sementa, L.; Medves, M.; Ramakrishna, G.; Fortunelli, A.; Oliver, A. G.; Dass, A. Crystal Structure of Au_{36-x}Ag_x(SPh-tBu)₂₄ Nanoalloy and the Role of Ag Doping in Excited State Coupling. *J. Phys. Chem. C* **2019**, 123, 29484–29494.
- (45) Kumara, C.; Gagnon, K. J.; Dass, A. X-Ray Crystal Structure of Au_{38-x}Ag_x(SCH₂CH₂Ph)₂₄ Alloy Nanomolecules. *J. Phys. Chem. Lett.* **2015**, *6*, 1223–1228.
- (46) Crasto, D.; Malola, S.; Brosofsky, G.; Dass, A.; Häkkinen, H. Single Crystal XRD Structure and Theoretical Analysis of the Chiral Au₃₀S(S-t-Bu)₁₈ Cluster. *J. Am. Chem. Soc.* **2014**, *136*, 5000–5005.
- (47) Chang, L.; Baseggio, O.; Sementa, L.; Cheng, D.; Fronzoni, G.; Toffoli, D.; Aprà, E.; Stener, M.; Fortunelli, A. Individual Component Map of Rotatory Strength and Rotatory Strength Density Plots As Analysis Tools of Circular Dichroism Spectra of Complex Systems. *J. Chem. Theory Comput.* **2018**, *14*, 3703–3714.
- (48) Herbst-Irmer, R.; Spek, A.; Schneider, T.; Sawaya, M. Crystal Structure Refinement: A Crystallographer's Guide to SHELXL; Oxford University Press, 2006; Vol. 8.
- (49) Guidez, E. B.; Mäkinen, V.; Häkkinen, H.; Aikens, C. M. Effects of Silver Doping on the Geometric and Electronic Structure and Optical Absorption Spectra of the Au_{25-n}Ag_n(SH)₁₈⁻ (n = 1, 2, 4, 6, 8, 10, 12) Bimetallic Nanoclusters. *J. Phys. Chem. C* **2012**, *116*, 20617–20624
- (50) Li, Q.; Wang, S.; Kirschbaum, K.; Lambright, K. J.; Das, A.; Jin, R. Heavily Doped $Au_{25-x}Ag_x(SC_6H_{11})_{18}^-$ Nanoclusters: Silver Goes from the Core to the Surface. *Chem. Commun.* **2016**, *52*, 5194–5197.
- (51) Bootharaju, M. S.; Joshi, C. P.; Parida, M. R.; Mohammed, O. F.; Bakr, O. M. Templated Atom-Precise Galvanic Synthesis and Structure Elucidation of a [Ag₂₄Au(SR)₁₈]⁻ Nanocluster. *Angew. Chem., Int. Ed.* **2016**, 55, 922–926.
- (52) Desireddy, A.; Conn, B. E.; Guo, J.; Yoon, B.; Barnett, R. N.; Monahan, B. M.; Kirschbaum, K.; Griffith, W. P.; Whetten, R. L.;

- Landman, U.; Bigioni, T. P. Ultrastable Silver Nanoparticles. *Nature* **2013**, *501*, 399–402.
- (53) Krause, L.; Herbst-Irmer, R.; Sheldrick, G. M.; Stalke, D. Comparison of Silver and Molybdenum Microfocus X-Ray Sources for Single-Crystal Structure Determination. *J. Appl. Crystallogr.* **2015**, 48, 3–10.
- (54) Dolomanov, O. V.; Bourhis, L. J.; Gildea, R. J.; Howard, J. A. K.; Puschmann, H. OLEX2: A Complete Structure Solution, Refinement and Analysis Program. *J. Appl. Crystallogr.* **2009**, *42*, 339–341.
- (55) Sheldrick, G. M. Crystal Structure Refinement with SHELXL. *Acta Crystallogr., Sect. C: Struct. Chem.* **2015**, *71*, 3–8.
- (56) Sheldrick, G. M. SHELXT Integrated Space-Group and Crystal-Structure Determination. *Acta Crystallogr., Sect. A: Found. Adv.* **2015**, *71*, 3–8.